European Polymer Journal 194 (2023) 112141

Contents lists available at ScienceDirect

European Polymer Journal

journal homepage: www.elsevier.com/locate/europolj

Impact of lignin source on the performance of thermoset resins

Iuliana Ribca [a,b], Benedikt Sochor [c], Marie Betker [c,d], Stephan V. Roth [b,c], Martin Lawoko [a,e], Olena Sevastyanova [a,e], Michael A.R. Meier [f,g], Mats Johansson [a,b,*]

[a] Wallenberg Wood Science Center (WWSC), Department of Fibre and Polymer Technology, KTH Royal Institute of Technology, Teknikringen 56-58, SE-100 44 Stockholm, Sweden
[b] Division of Coating Technology, Department of Fibre and Polymer Technology, KTH Royal Institute of Technology, Teknikringen 48, SE-100 44 Stockholm, Sweden
[c] Deutsches-Elektronen Synchrotron (DESY), Notkestraße 85, 22607 Hamburg, Germany
[d] Division of Fibre Processes, Department of Fibre and Polymer Technology, KTH Royal Institute of Technology, Teknikringen 58, 100 44 Stockholm, Sweden
[e] Division of Wood Chemistry and Pulp Technology, Department of Fibre and Polymer Technology, KTH Royal Institute of Technology, Teknikringen 56, SE-100 44 Stockholm, Sweden
[f] Institute of Organic Chemistry (IOC), Materialwissenschaftliches Zentrum MZE, Karlsruhe Institute of Technology (KIT), Straße am Forum 7, 76131 Karlsruhe, Germany
[g] Institute of Biological and Chemical Systems—Functional Molecular Systems (IBCS-FMS), Karlsruhe Institute of Technology (KIT), Hermann-von-Helmholtz-Platz 1, 76344 Eggenstein-Leopoldshafen, Germany

ARTICLE INFO

Keywords:
Hardwood lignin
Solvent fractionation
Allylation
Thiol-ene thermosets
Wide-angle X-ray scattering
π-π stacking interactions

ABSTRACT

A series of different technical hardwood lignin-based resins have been successfully synthesized, characterized, and utilised to produce thiol-ene thermoset polymers. Firstly, technical lignin was fractionated and allylated, whereafter it was crosslinked with a trifunctional thiol. Structural and morphological characteristics of the lignin fractions were studied by ^{1}H NMR, ^{31}P NMR, SEC, FTIR, DSC, TGA, and WAXS. The hardwood lignin fractions have a high content of C_5-substituted OH groups. The WAXS studies on lignin fractions revealed the presence of two π-π stacking conformations, sandwiched (4.08–4.25 Å) and T-shaped (6.52–6.91 Å). The presence of lignin superstructures with distances/sizes between 10.5 and 12.8 Å was also identified. The curing reaction of the thermosets was investigated by RT-FTIR. Almost all thermosets (excepting one fraction) reached 95% of the thiol conversion in less than 17 h, revealing the enhanced reactivity of the allylated hardwood lignin samples.

The mechanical properties of the thermosets were investigated by DMA. The curing performance, as well as the final thermoset properties, have been correlated to variations in chemical composition and morphological differences of lignin fractions. The described results clearly demonstrate that technical hardwood lignins can be utilized for these applications, but also that significant differences compared to softwood lignins have to be considered for material design.

1. Introduction

Thermosetting polymers are cross-linked polymer networks with attractive thermo-mechanical properties for advanced applications. These materials are, for example, used in automotive and aerospace parts, electronic materials, adhesives, and coatings [1]. Most of these high-performance thermosets contain aromatic structures to obtain a high modulus. The aromatic monomers used, e. g. bisphenol A, terephthalic acid, phthalic acid, or phenol, are mainly derived from fossil resources. Some of these monomers are also debated with respect to adverse effects on human endocrine system, e. g. bisphenol A [2–4]. Nowadays, a lot of research is focused on finding bio-based and eco-friendly replacements for these constituents [5]. For example, extensive research on sugar-based monomers, such as furan dicarboxylic acid, to replace terephthalic acid used in polyethylene terephthalate (PET) has been described [6,7]. Another abundant source of aromatics in nature is lignin, which has been exploited both as monomeric entities as well as oligomeric building blocks [8–14]. A wide variety of different technical lignins are available, depending on species origin and retrieval processes and although extensively investigated, it is still not clear how these different lignins affect the final properties when used in polymeric materials [15].

* Corresponding author at: Wallenberg Wood Science Center (WWSC), Department of Fibre and Polymer Technology, KTH Royal Institute of Technology, Teknikringen 56-58, SE-100 44 Stockholm, Sweden.
E-mail address: matskg@kth.se (M. Johansson).

https://doi.org/10.1016/j.eurpolymj.2023.112141
Received 27 March 2023; Received in revised form 2 May 2023; Accepted 7 May 2023
Available online 11 May 2023

Lignin is the most abundant aromatic biopolymer found in nature [16]. It acts as a binder between cellulose and hemicellulose in the plant cell wall and confers strength and hydrophobicity to the lignocellulosic matrix. Lignin has a complex structure resulting from radical coupling and cross-coupling of the three main monolignols: p-coumaryl, coniferyl, and sinapyl alcohols. These building blocks correspond to p-hydroxyphenyl H, guaiacyl G, and syringyl S phenylpropanoid units in lignin network (Scheme S1, adapted from [17]). The composition and distribution of these units (building blocks) vary among different plant species. For example, lignins from gymnosperm (softwood) are mostly composed of G units and have a low level of H units, whereas lignins from dicotyledonous angiosperm (hardwood) are composed of G and S units, and also some traces of H units. Lignins from grasses (monocots) have a similar content of G and S units and more H units if compared to softwood and hardwood lignins [17]. Lignin inter-unit linkages are formed through radical coupling. The most common inter-unit linkages are the β-O-4, β-5, β-β, 5–5, 5-O-4, and β-1. The monomer composition determines the inter-unit linkage frequencies. As a consequence, softwood lignins have a higher content of β-5, 5–5, and 5-O-4 linkages than hardwood and grass lignins, due to the higher relative abundance of G units, which are free of methoxy groups at C_5 position. In contrast, the C_5 position in S units is occupied by a methoxy group, so it is not available for the coupling [16,17].

Large quantities of technical lignin are produced by the pulp and paper industries every year [18]. Despite its availability and relatively low price, lignin utilization in high value-added materials is limited because of its heterogeneity and structural complexity. It is possible to obtain more homogeneous lignin fractions by using solvent fractionation [19–22], membrane filtration [23,24], or pH-dependent precipitation [25]. The lignin reactivity can also be enhanced by chemically modifying its functional groups, for example phenolic, aliphatic, or carboxylic acid hydroxyl groups [26]. One way of modifying the hydroxyl groups is by introducing an allyl functionality to lignin [27–31]. The modified lignin fractions can be used as a thiol-ene thermoset precursors [32–34].

The purpose of this work was to evaluate how the lignin source affects the material properties of thereof derived thermosets in, softwood versus hardwood Kraft lignins. A sequential solvent fractionation approach was used to obtain more homogeneous Kraft hardwood lignin fractions with narrow dispersity [19]. Subsequently, mild reaction conditions were used to introduce allyl functionalities into the lignin polymer [28,35]. The highly functionalized lignin was then cross-linked with a trifunctional thiol cross-linker (Scheme S2, adapted from. The curing performance and the thermo-mechanical properties of the obtained thiol-ene thermosets were studied and compared with the corresponding softwood-based thermosets described in literature in order to understand how the lignin source is influencing these properties. The results showed a significant difference in reactivity (real time Fourier transform infrared spectroscopy), morphology (wide angle X-ray scattering), and physical properties (differential scanning calorimetry, dynamic mechanical analysis) depending on the initial lignin source.

2. Experimental section

2.1. Materials

Hardwood (*Eucalyptus grandis*) LignoBoost Kraft lignin was extracted from Kraft pulping liquor according to LignoBoost technology [36]. Ethyl acetate (EtOAc, ≥99%), ethanol (EtOH, ≥99.8%), methanol (MeOH, ≥99.8%), acetone (≥99.5%), and hydrochloric acid (HCl, 37%) were purchased from VWR International. Diallyl carbonate (DAC, 99%), tetrabutylammonium bromide (TBAB, 98%), cyclohexane (99.5%), and trimethylolpropane tris(3-mercaptopropionate) (3TMP, ≥95%) were purchased from Sigma-Aldrich. Magnesium sulfate ($MgSO_4$, 99%) was purchased from Thermo Scientific Chemicals. Silicone molds were prepared using silastic T-2 base/curing agent (10:1 w/w) which were acquired from Dow Corning. All other chemicals were purchased from Sigma-Aldrich.

2.2. Procedures

2.2.1. Lignin purification and sequential solvent fractionation

Hardwood lignin was washed with deionized water in order to remove inorganic impurities [33,34]. ≈10 g of lignin powder was mixed with 200 mL of deionized water. The mixture was magnetically stirred at 60° for 2 h. Afterwards, lignin was filtrated using a sintered funnel (grad 4). The procedure was repeated until the pH of the filtrate was above 5.5 (3–4 times). The washed lignin (HW-Initial) was dried in a vacuum oven at 50 °C for 24 h. The recovery yield of washed lignin was determined to be 80 ± 1%.

Subsequently, the washed lignin was sequentially solvent fractionated [19,33,34]. An amount of 10 ± 1 mg of washed lignin was added to 100 mL of EtOAc in a 250 mL glass beaker. The mixture was stirred at room temperature for 2 h and afterwards filtrated through a grade 3 Munktell filter paper. The EtOAc soluble fraction was rotary evaporated. Both fractions, EtOAc soluble and insoluble were dried in the vacuum oven at 50 °C for 24 h. Afterwards, the EtOAc soluble fraction was redissolved in acetone, precipitated in 200 mL of deionized water, and freeze-dried. The same extraction procedure was then repeated on the respective insoluble fraction with EtOH, MeOH, and acetone. The lignin to solvent ratio was 1:10 (g/mL) in all cases. Five fractions were obtained after the extraction procedure and were denoted HW-EtOAc, HW-EtOH, HW-MeOH, HW-Acetone, and HW-Insoluble.

2.2.2. Allylation of hardwood lignin samples

An amount of 1 g (≈6.0 mmol of various OH groups/g of lignin) of HW-Initial and the obtained five fractions were placed in separate 10 mL pressure vials. TBAB (1 eq/OH groups, ≈1.9 g) and DAC (3 eq/OH groups, ≈2.6 g) were added into the vials. The pressure vials were sealed and magnetically stirred at 120 °C for 5 h. The reaction mixture was left to cool to room temperature. After cooling, it was dissolved in EtOAc and placed in a separatory funnel. The liquid–liquid extraction (EtOAc/water) was used to recover TBAB from the mixture. Subsequently, the water was rotary-evaporated and TBAB was dried in the vacuum oven. The recovery yield of TBAB was 88 ± 3%. $MgSO_4$ was used to dry the organic phase. Then, the organic phase was filtrated, concentrated by using a rotary evaporator to 5 mL and precipitated into 200 mL of cold cyclohexane. The obtained lignin was filtered (Munktell filter paper, grade 3), washed with cyclohexane, and dried in the vacuum oven at 50 °C for 24 h [29,34]. The obtained allylated lignin samples were denoted: DAC-HW-Initial, DAC-HW-EtOAc, DAC-HW-EtOH, DAC-HW-MeOH, DAC-HW-Acetone, and DAC-HW-Insoluble.

2.2.3. Preparation of Lignin-Based thermosets

For each free-standing sample, around 40 mg of allylated lignin was used. The thiol cross-linker was added into the vial and everything was dissolved in 150 mL of EtOAc. The thiol:ene molar ratio was 1:1, and the thermoset compositions are presented in Table S7. The mixture was poured into a silicone mold and left in the fume hood overnight to allow solvent evaporation and film formation. Subsequently, the mold was placed into an oven and cured at 125 °C for 25 h (the resin prepared from DAC-HW-EtOAc was cured at 125 °C for 40 h). The free-standing samples were removed from the molds and stored in petri dishes [28,32–34]. The samples dimensions were ≈12 mm × 5.2 mm × 0.10 mm. The obtained thermoset samples were denoted T3-DAC-HW-Initial, T3-DAC-HW-EtOAc, T3-DAC-HW-EtOH, T3-DAC-HW-MeOH, T3-DAC-HW-Acetone, and T3-DAC-HW-Insoluble.

2.2.4. Curing performance of lignin-based thermosets

The curing performance of the thermoset formulations was monitored using real time FTIR. A drop of the resin solution (previously described) was added to a pre-heated attenuated total reflection (ATR)

accessory, equipped with a diamond crystal. The FTIR spectra were recorded as described in the methodology section.

2.3. Characterization techniques

2.3.1. Ash content

The ash content of lignin samples was measured as described in the T 211 om-02 method (Ash in wood, pulp, paper and paperboard: combustion at 525 °C). An amount of ≈0.50 g of lignin samples (before and after washing) were firstly dried and afterwards placed in a muffle furnace (M9-1200). First, samples were kept at 250 °C for 30 min and then they were kept at 525 °C for 5 h. The results represent an average of three measurements.

2.3.2. Inductively coupled Plasma-Optical emission spectroscopy (ICP-OES)

Thermo Scientific iCAP 6000 instrument was used to determine the inorganics in lignin samples before and after washing procedure. All samples were prepared by following the US EPA SW-846 method 3050A, with some modifications [33].

2.3.3. Size exclusion chromatography (SEC)

Size exclusion chromatography was used to determine the molar mass (number-average, M_n and weight-average molar mass, M_w) and dispersity ($Đ$) of lignin samples. 2 mg of sample were completely dissolved in 2 mL of the elution solvent (hexafluoro-2-propanol, HFIP with 0.1 wt% potassium trifluoroacetate) and filtered through a syringe filter of 0.45 μm. The solvent flow was 0.40 mL min^{-1} at 35 °C. The measurements were performed on a Tosoh EcoSEC HLC-8320 SEC system equipped with a three-column system: PSS PFG Micro precolumn (10000, 1000 Å, and 100 Å). Methyl methacrylate standards were used as an internal standard with a molar mass range of 102–981 kg mol^{-1}.

2.3.4. Proton and phosphorus nuclear magnetic resonance spectroscopy (^1H and ^{31}P NMR)

The spectra were obtained using a Bruker Avance III HD 400 MHz instrument with a BBFO probe equipment with a Z-gradient coil. The spectra were phase and baseline, (Bernstein Polynomial Fit) corrected. For ^1H NMR, ≈20 mg of lignin samples were dissolved in 550 μL DMSO-d_6. The relaxation delay was set to 5 s, with a total number of 128 scans and acquisition time of 4.9 s. For ^{31}P NMR, ≈25 mg of lignin samples were mixed with 100 μL of anhydrous pyridine and 100 μL of dimethyl formamide. After complete dissolution, 50 μL solution of internal standard (≈30 mg of n-hydroxy-5-norbornene-2,3-dicarboximide, 97%, and ≈2.5 mg of chromium (III) acetylacetonate were dissolved in 500 μL of anhydrous pyridine) were added and everything was mixed thoroughly. 150 μL of phosphitylation reagent (2-chloro-4,4,5,5-tetramethyl-1,3–2-dioxaphospholane, 95%) were added and the formed precipitate was dissolved in 400 μL deuterated chloroform. The NMR spectra were recorded 20 min after the preparation. The data was acquired with an inverse gated decoupling pulse (zgig30) and an acquisition time of 1.67 s, a relaxation delay of 10 s, and a number of scans set to 128 [33,37].

2.3.5. Fourier transform infrared spectroscopy (FTIR) and real time FTIR (RT-FTIR)

PerkinElmer Spectrum 100 system with an ATR accessory, equipped with a diamond crystal, and a temperature control unit (Specac, Heated Golden Gate Controller) was used to characterize the lignin samples. FTIR spectra were acquired at room temperature, by averaging 16 scans, from 4000 to 600 cm^{-1}, with a resolution of 4 cm^{-1}. RT-FTIR measurements were performed at 125 °C and a new scan was acquired every minute. All spectra were normalized to the 1509 cm^{-1} signal (1501 cm^{-1} for thermosetting resins), corresponding to stretching vibration of aromatic C = C, and baseline corrected by using Spectrum software [38]. Thiol conversion was determined by monitoring the decrease in RT-FTIR absorption intensity of the S-H signal (2607–2533 cm^{-1}) [39].

2.3.6. Differential scanning calorimetry (DSC)

DSC thermograms of lignin samples were recorded on a Mettler Toledo DSC1 instrument. An amount of ≈10 mg of each sample was placed in a 100 μL aluminium crucible and covered with pierced lid. The samples were first heated to 105 °C (maintained at this temperature for 20 min) and afterwards cooled to –40 °C (maintained at this temperature for 10 min). Then, the samples were heated up to 250 °C. The heating/cooling rate was 10 °C/min. The glass transition temperature (T_g) was calculated as the midpoint from the second heating run.

2.3.7. Thermogravimetric analysis (TGA)

TGA was performed on a Mettler Toledo TGA/DSC1 instrument. An amount of ≈10 mg of lignin sample was placed in a 70 μL ceramic crucible. Firstly, samples were heated to 30 °C and kept for 10 min, afterwards they were heated up to 800 °C and kept for another 10 min. The heating rate was set to 10 °C/min and the nitrogen flow 50 mL/min. $T_{5\%}$ and $T_{50\%}$ indicate when 5%, respectively 50% weight loss was observed.

2.3.8. Dynamic mechanical analysis (DMA)

DMA was performed on a DMA Q800 instrument in tensile mode. Samples were cooled to –55 °C (held for 5 min) and then heated up to 205 °C with a heating rate of 3 °C/min. The preload force was set to 0.01 N, with a force track of 125%, a frequency of 1 Hz, and a strain of 0.1%. The samples dimensions were ≈12 mm × 5.2 mm × 0.10 mm. Storage modulus (E'), loss modulus (E''), and tan δ were continuously recorded as a function of temperature. T_g of the thermosets was reported as maximum of tan δ.

2.3.9. Wide-Angle X-ray scattering (WAXS)

Wide angle X-ray scattering measurements were performed at beamline P03 (PETRA III, Hamburg, Germany) [40]. For the measurements, the powders were pressed with a hydraulic laboratory press into pellets (diameter = 13 mm, thickness = 1 mm) while the lignin thermosets (12 mm × 5.2 mm × 0.10 mm) were measured as is. A LAMBDA 9 M (X-spectrum, Hamburg, Germany) detector was used, with a fixed X-ray wavelength of 1.048 Å (E = 11.83 keV). The sample to detector distance (SDD) was set to 21 cm with a beam size of 25 × 25 $μm^2$. To avoid beam damage by the X-rays, the radiation dose was spread by scanning on 100 different positions over a region of 2 × 2 mm^2 with an illumination time of 1 s each. The acquired images were summed up and reduced to 1D scattering profiles. The data reduction was done by applying azimuthal integration and normalization as described in literature followed by a background subtraction (air scattering) [41]. The scattering profiles show the radially averaged intensities over the scattering vector $q = (4\pi/\lambda) \sin\theta$ where λ is the X-ray wavelength and θ is the scattering angle, measured from the point where the primary beam hits the detector. The scattering profiles were fitted by using a combination of Gaussian functions. The obtained peak position q^* in reciprocal space were then re-calculated to give the so-called D-spacing ($D = 2\pi/q^*$). The D-spacing is related to the distances and sizes of repeating features in real-space.

2.3.10. Atomic force microscopy

Atomic force microscopy measurements were conducted at room temperature, in air, using the Bruker Multi Mode 8 in Peak Force QNM mode. A silicon tip on nitride lever (T: 650 nm, L: 115 nm, f: 70 kHz, model scanasyst-air) with reflective Al coating on the back side was used. The images were taken at an average scan rate of 0.7 Hz. Analysis was made using NanoScope Analysis 1.50 software (Bruker Corporation).

3. Results and discussion

The aim of this work was to investigate the role of the lignin source on the structure–property relationship of previously described thermosets [34]. The effect of fractionation process and cross-linking reaction on lignin morphology, at nano-level, was investigated.

3.1. Hardwood lignin fractionation

In this study, Eucalyptus hardwood lignin, from the Kraft process, was used. The efficiency of the purification process was assessed by evaluating the ash and inorganics content in lignin samples before and after the washing processes. It was observed that the ash content decreased after the washing from 0.6 ± 0.1% to 0.3 ± 0.1%. At the same time, the content of S, Na, and Ca also decreased (see Table S1). The higher content of S and Na in the initial samples could be a result of the Kraft pulping process, where sodium sulphide (Na_2S) and sodium hydroxide (NaOH) are used [36,42,43].

Eucalyptus hardwood lignin was refined by using sequential solvent fractionation approach. Four solvents (EtOAc, EtOH, MeOH, and acetone) were involved in this process and five fractions, with tuneable properties, were obtained (including the residual fraction). The M_n, M_w, and $Đ$ data of the initial lignin and obtained fractions are shown in Figure S1 and Table S2. In previous studies, it was showed that the M_w for hardwood lignin samples was lower compared with the softwood samples [22]. Also, the M_w increased from HW-EtOAc (650 g/mol) to HW-Insoluble (9700 g/mol). The same trend was previously observed by Duval et al. [19] for softwood Kraft lignin and by Gioia et al. for hardwood Kraft lignin when subjected to solvent fractionation approach. At the same time, the $Đ$ for all recovered fractions was lower than the $Đ$ for the HW-Initial. The yields of the fractionation process were reported in Table S2. It was noted that the content of residual hardwood fraction (HW-Insoluble) was lower (around 14%) than the content of residual softwood fraction (34%). This is due to the fact that hardwood lignin is more soluble in EtOAc, thus the content of HW-EtOAc was higher (≈37%) [22,33].

The hydroxyl groups represent potential targets for chemical modification of lignin. Also, the OH groups play a crucial role in the formation of inter- and intramolecular hydrogen bonds. Thus, the characterization of OH groups in lignin is crucial. The qualitative (Figure S2) and quantitative (Fig. 1) analysis of OH-groups were studied by ^{31}P NMR. Different OH groups were identified: aliphatic, C_5-substituted (e. g. 5–5, 4-O-5), guaiacyl, p-hydroxyphenyl, and carboxylic acid OH. It was observed that the aliphatic, p-hydroxyphenyl, and guaiacyl OH groups content in hardwood is lower than in softwood. Also, the fraction of C_5-substituted OH is much higher in hardwood (2.35–3.99 mmol/g) [22,33,34]. This is due to the monolignol composition of native hardwood lignin, which has a high content of syringyl units [44,45]. Overall, the total OH content in hardwood (6.1–6.8 mmol/g) was lower than in softwood (6.5–7.4 mmol/g) [34] if comparing the same fractions. The content of aliphatic OH groups increased from HW-EtOAc to HW-Insoluble (excepting the HW-Acetone). Moreover, the C_5-substituted and guaiacyl OH groups content decreased from HW-EtOAc to HW-Insoluble. The higher phenolic OH groups content in HW-EtOAc fraction is due to the extensive cleavage of β-O-4 linkage during the pulping process and the generation of phenolic OH. In this way, more phenolic OH are present in the lower molecular weight fractions [45].

As previously stated, the main difference between hardwood and softwood lignin is the high content of syringyl units present in hardwood lignin. This was also confirmed by FTIR spectroscopy (Figure S3). The new signals at 1324 cm^{-1} and 1109 cm^{-1} present in hardwood lignin were attribute to the C–H vibrations in syringyl units. It was also noticed that the intensity of the signal at 1265 cm^{-1} corresponding to the C-O stretching vibration in the guaiacyl unit was drastically reduced in hardwood lignin [46–48].

DSC analysis of all the different fractions revealed a T_g between 111 and 193 °C as can be seen in Figure S6. It was also observed that chemical changes start to occur above T_g i. e. the DSC traces become very irregular. This is furthermore seen in the TGA thermograms (Figure S5). All lignin samples showed a similar degradation profile, where half of their initial mass was lost between 429 and 509 °C (Table S3). It is interesting to note that HW-EtOAc showed less mass loss between 150 °C and 250 °C. This might be due to the higher guaiacyl

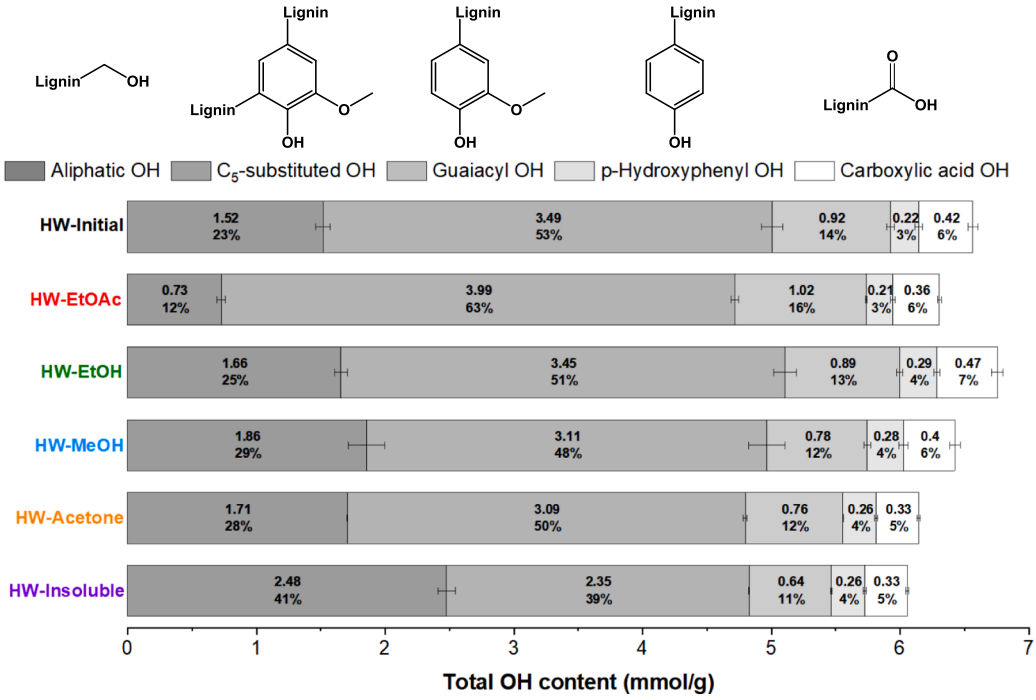

Fig. 1. Chemical structure and content of OH functionalities in HW-Lignin samples determined by ^{31}P NMR. Data is presented as relative percentages for each sample as well as absolute values in mmol of various OH groups/g of lignin.

content in this fraction. Guaiacyl units tend to condense at the free C_5-position, creating C–C linkages, which are more thermally stable [43].

The fractionation approach allowed us to obtain lignin fractions with different features in terms of molecular weight, dispersity, content of OH functionalities, and thermal behaviour. Furthermore, by targeting the OH groups, the reactivity of lignin samples can be enhanced and they can be used for synthesis of different resins.

3.2. Allylation of hardwood lignin

It is possible to improve lignin's combability with other materials and enhance its mechanical properties by chemically modifying it [49]. In this study, allyl functionalities were introduced to the different lignin samples by using diallyl carbonate. A simplified representation of the allylation reaction is showed in Scheme 1. The efficiency of the reaction was assessed by SEC, FTIR, ^{1}H NMR, ^{31}P NMR. SEC measurements were performed for all modified lignin samples and the results are shown in Figure S7 and Table S4. The measured M_w increased by at least a factor of two for all samples after the incorporation of allyl functionalities. This increase corresponds to an increased hydrodynamic radius which not only depend on molecular weight, but also the solvent-polymer interaction that changes when transforming OH groups to allyl moieties. Hence the values should be considered as trends, rather than absolute values. FTIR spectra (Figures S8–S9) show a decrease in the characteristic OH stretching vibration signal between 3670 and 3150 cm^{-1} in the modified lignins. This is due to OH groups consumption during the allylation reaction. Also, a new signal was observed at 1725 cm^{-1} corresponding to the carbonyl C = O stretching vibration resulting from allyl carbonates [50]. Four more signals were identified in modified lignin at 3077, 1649, 985, and 921 cm^{-1} that correspond to the vibrations of allyl functionalities [27,29,34].

In the ^{1}H NMR, the appearance of three new signals between 6.52 and 4.05 ppm confirm the successful integration of the allyl functionalities to lignin (Figures S4 and S10) [29]. ^{31}P NMR studies indicated that all phenolic and carboxylic OH groups were almost completely allylated, meanwhile the aliphatic OH groups were just partially allylated (Figure S11). The conversion for different phenolic OH groups on average was $\geq$ 97%, for carboxylic acid OH groups it was $\geq$ 91%, and for aliphatic OH groups it was between 45 and 70%. In previous studies [29,34], it was showed that the phenolic OH groups were converted into allyl aryl ethers, the carboxylic acid OH were converted into allyl esters, and aliphatic OH groups were partially converter into allyl carbonates and partially into allyl ethers [29,34]. Further analytical experiments are required in order to determine the amount of allyl ethers or allyl carbonates installed at aliphatic OH groups. Overall, the percentage and the total amount of allylated aliphatic OH groups in hardwood lignin samples was relatively the same as in softwood (Table S5) [34]. The content of allylated aliphatic OH groups in all fractions was between 0.4 and 1.8 mmol/g. All modified lignin samples had an allyl content on average, comprised between 5.1 and 5.9 mmol/g. These findings suggested that the high content of syringyl units does not affect the reactivity of the phenolic OH groups (no steric hindrance from the methoxy groups).

From the DSC analysis it was observed that the T_g of the allylated hardwood lignin samples was between 61 and 112 °C (Figure S12). These values are significantly lower compared with the same samples before allylation. These results revealed the importance of the hydrogen bonding interactions on the lignin thermal properties. It was also observed that the T_g of DAC-HW-Lignin samples was higher than the T_g of the DAC-SW-Lignin samples [34]. From the TGA analysis it was noticed that the modified lignin samples start to degrade at higher temperature compared to unmodified lignin samples ($T_{5\%}$ is higher for the modified samples, see Table S6). Allylated lignin samples start to degrade at around 200 °C as can be seen in Figure S13. The mass loss between 200 and 325 °C it is more pronounced in allylated lignin and can be attributed to the degradation of the newly introduced functionalities.

3.3. Study of the curing process of Lignin-Based thermosetting resins

Trimethylolpropane tris(3-mercaptopropionate) thiol was used as cross-linking agent for the allylated lignin samples. This cross-linking agent is a trifunctional thiol available at industrial scale. The relative content of lignin and thiol is influenced by the total amount of allyl functionalities. Accordingly, the lignin content was between 56 and 62 wt%, therefore ≈3–4% higher than in previous study on softwood lignin (Table S7) [34].

The curing process was followed by RT-FTIR. At the beginning of the reaction, the thiol (2570 cm^{-1}) and allyl (1642 cm^{-1}) signals were distinct. Already after ≈1h, a significant decrease of these signals was noticed. The thiol consumption for T3-DAC-HW-EtOH over time is shown in Figure S14. Toward the end of the curing process, the thiol signal completely disappeared, suggesting that the functional groups reacted and the cross-linked networked was formed. The FTIR spectra before and after curing are shown in Figures S15–16. Surprisingly, it was found that the curing reaction was significantly faster compared with the previous study on softwood lignin (Table S8 and Fig. 2) [34]. The hardwood lignin resins reached 20% of thiol conversion in less than 0.8 h (except for T3-DAC-HW-EtOAc, 3.7 h), meanwhile for softwood it was reached after less than 3 h (except for T3-DAC-HW-EtOAc, 7.6 h). At the same time 50% of thiol conversion for hardwood was reached between 0.7 and 2.7 h (except for T3-DAC-HW-EtOAc, 13.9 h) and for softwood it was between 8.0 and 14.2 h (except for the T3-DAC-SW-EtOAc, 20.6 h). It is not clear why the curing reaction for T3-DAC-HW-EtOAc is significantly slower, but it was noticed that the total aryl allyl ethers content of this fraction is much higher. At the same time, the curing reaction for the T3-DAC-HW-Insoluble was faster and it also corresponds to the lowest aryl allyl ethers content. It can thus be suggested that the aryl allyl ethers play an important role on the curing performance of these lignin-based thermosets. Overall, this study revealed that the allylated hardwood lignin has enhanced reactivity. It is proposed to be due to the better accessibility of the allyl functionalities, suggesting a more open

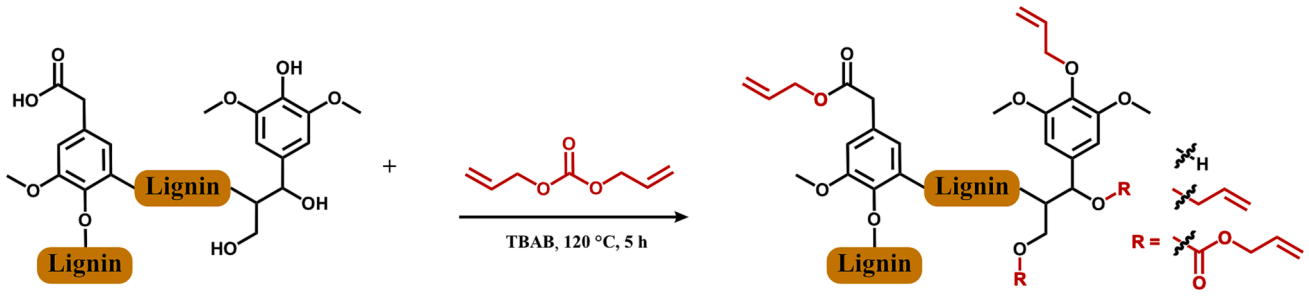

Scheme 1. Simplified representation of the allylation reaction with DAC of HW-Lignin samples. It was assumed that all phenolic and carboxylic acid OH were fully functionalized.

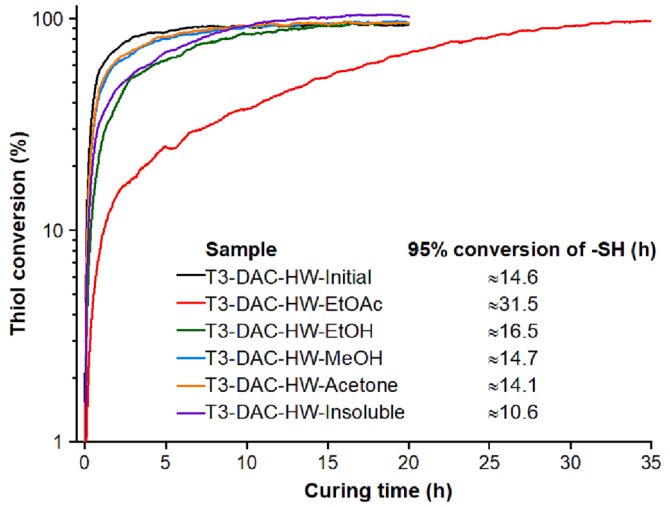

Fig. 2. RT-FTIR data collected during the thermal curing of allylated hardwood lignin samples at 125 °C. The conversion of thiol signal (2607–2533 cm^{-1}) is shown as a function of time.

structure in hardwood lignin, i. e. less condensed lignin backbone, but also lower M_w of the hardwood lignin fractions.

3.4. Morphological characterization of lignin samples

The effect of π-π stacking interactions, on different aromatic systems, has been widely studied. π-π stacking interactions are referring to the interactions between aromatic rings containing π systems [51,52]. They are reversible and with different geometric configurations. π-π stacking interactions, hydrogen bonding and other noncovalent interactions play an important role in self-assembly, superstructure formation, and stability of the chemical systems [53].

Lignin is a multiaromatic polymer with a high content of OH groups. Various studies showed that lignin can form hydrogen bonds and π-π stacking interactions [20,54]. The presence of π-π stacking interactions can be determined by X-ray scattering techniques (WAXS). Previously, two π-π stacking conformations were identified in lignin samples: sandwiched (combined parallel displaced and cofacial parallel stacked) and T-shaped π-π stacking interactions [32–34]. The same configurations were observed in the present study in hardwood lignin fractions and thermoset samples (Figures S17–18).

Comparing with previous data, it was noticed that the distances of sandwiched π-π stacking interactions (D_3) in softwood and hardwood samples were the same (between 4.1 and 4.3 Å). Meanwhile, the distances of T-shaped π-π stacking interactions (D_2) were shifted with 0.5–1.0 Å in hardwood samples, with distances between 6.5 and 6.9 Å (the real-space data can be seen in Table 1 and the reciprocal-space data can be seen in Table S9) [34]. This indicates that the lignin side chains, the different linkages, and the distribution of various monolignol units play an important role in lignin conformation and morphology. The main difference between softwood and hardwood is the presence of syringyl units. This could thus be an indication that the methoxy groups expand the distance between the aromatic rings and create a more open structure [55]. The T-shaped stacking interactions are the dominant conformation in lignin samples, which account for 76–80% of the sum of D_1, D_2, and D_3 (Table S10).

Another signal, D_1, with a longer distance/sizes (between 10.5 and 12.8 Å) was identified in all lignin samples. It was suggested that this signal indicates the presence of lignin superstructures, which can be intra- or intermolecular [34].

The presence of π-π stacking interactions was also identified in the thermosetting samples, with T-shaped stacking interactions as a dominat conformation (Figure S19-21, Table S12). The real-space data can be seen in Table 2 and the reciprocal-space data can be seen in Table S11. The D_1 signal in the thermosets increased (14.0–17.5 Å) and at the same time a new signal D_4, at around 3.4 Å, was indentified (Figures S19–21). The D_1 signal intensity significantly varies between the different thermoset films. This implies that the formation of these superstructures is affected by the film formation process. This process is initially dominated by physical drying until the solvent is evaporated. Then a chemical cross-linking take place, which eventually locks the structure. Full details on this process is still under investigation to allow for a complete understanding. The D_4 signal was proposed to be related to the thioether organized structures [34]. The same thiol-cross-linker was used in the present study and finding similar distances/sizes in both cases suport this finding. $D_{II\ order\ x}$ (x = 3 or 4) were attributed to the second order signals of D_x. These signals represent an interference pattern and indicate a very well-ordered system [34]. The increase in the D_3 signal distances/sizes in the films also indicates a more open structure. It is still not fully clear how and to which extent π-π stacking interactions are affecting the lignin properties.

3.5. Mechanical properties of the thermosets

Thermo-mechanical properties of the lignin-based thermosets were evaluated by DMA (Fig. 3 and Figure S22). The DMA was performed on fully cured samples. The hardwood lignin-based thermosets showed a storage modulus of 2.2–3.6 GPa at −50 °C. All measured hardwood lignin thermosets showed a T_g ranging on average between 99 and 125 °C, which is significantly higher than the corresponding softwood thermosets by 8–30 °C. A number of different structural features, such as cross-link density, polarity, and chain rigidity affect the T_g of a thermoset. The structure of hardwood lignin is dominated by syringyl units, which means that the C_5-position is ocuppied by a methoxy group. The presence of the methoxy group will make hardwood lignin less condensed compared to softwood, i. e. less branched. It will also introduce mobility restrictions around the allyl aryl ether bond due to steric hindrance. It has furthermore been shown that technical lignins from hardwood (Eucalyptus grandis) retain more of flexible β-O-4 linkages compared to softwood lignin [56]. Another difference between the sofwood and hardwood thermosets in the present study is that the

Table 1
Repeating features within hardwood lignin samples determined by WAXS. The standard deviation for all samples was <0.1 Å.

Sample	$D_{1\ max}$ (Å)	$D_{2\ max}$ (Å)	$D_{3\ max}$ (Å)	$D_{II\ order\ 3}$ (Å)
HW-Initial	10.47	6.66	4.14	2.34
HW-EtOAc	10.47	6.52	4.16	2.26
HW-EtOH	10.47	6.75	4.25	2.3
HW-MeOH	10.47	6.87	4.24	2.33
HW-Acetone	12.82	6.91	4.08	2.23
HW-Insoluble	10.47	6.83	4.18	2.37

Table 2
Repeating features within hardwood lignin-based thermosets determined by WAXS. The standard deviation for all samples was <0.1 Å.

Sample	$D_{1\ max}$ (Å)	$D_{2\ max}$ (Å)	$D_{3\ max}$ (Å)	$D_{4\ max}$ (Å)	$D_{II\ order\ 3}$ (Å)	$D_{II\ order\ 4}$ (Å)
T3-DAC-HW-Initial	17.45	7.15	4.57	3.38	2.24	1.76
T3-DAC-HW-EtOAc	N/A					
T3-DAC-HW-EtOH	13.95	6.27	4.36	3.40	2.24	1.76
T3-DAC-HW-MeOH	14.09	6.12	4.35	3.41	2.24	1.76
T3-DAC-HW-Acetone	16.80	7.10	4.63	3.40	2.24	1.76
T3-DAC-HW-Insoluble	14.37	6.24	4.37	3.40	2.24	1.76

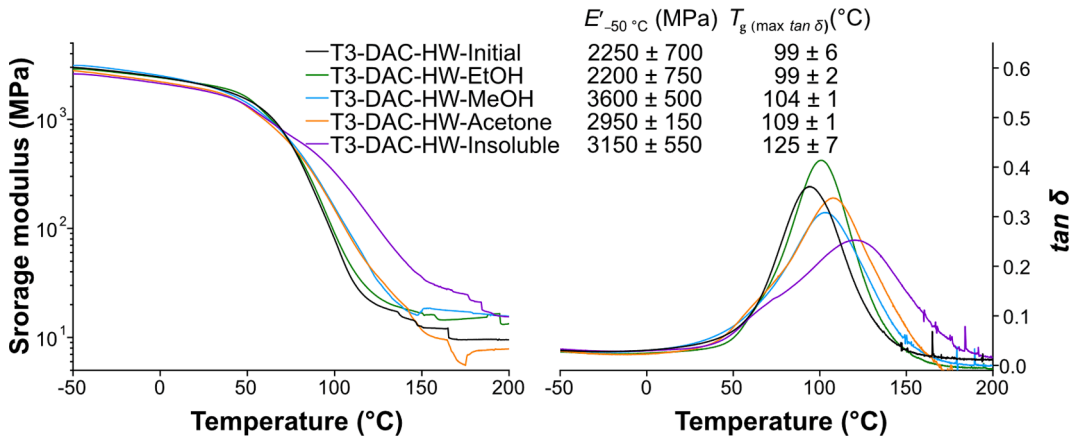

Fig. 3. Representative DMA curves of T3-DAC-HW-Lignin samples were the storage modulus (E') is shown on the left and tan δ on the right.

hardwood thermosets have a lower functionality leading to a slightly lower crosslink density. This also means that the hardwood thermosets have higher lignin content and less of flexible thioether bonds as well as leading to a difference in polarity. The combination of all these differences in structural features result in the observed differences in T_g. All thermosets showed a good thermal stability, with no degradation up to 220 °C and comparable with other lignin-based thiol-ene thermosets (Table S13, Figure S23) [32–34].

The lignin-based thermosets were also characterized by AFM (Figure S24). All films showed a similar morphology at the micrometer scale, with a surface roughnes between 0.40 and 0.65 nm (Table S14). This indicates that the differences in their mechanical properties are not related to morphology differences at the micrometer scale.

4. Conclusions

This study provided insightful information on how the lignin source influence thereof derived thermosets. The hardwood-based resins exhibited a high reactivity towards crosslinking with thiols. This was related to the less condensed and more open lignin structure in hardwood lignins. The mechanical properties of the lignin-based thermosets are influenced by the combination of the cross-link density, thioether content, polarity, and back-bone rigidity. By changing these parameters, it is possible to obtain thermosets with different properties. To conclude, hardwood lignin is a feasible alternative to softwood lignin with respect to material performance, but there are differences to consider.

Author Contributions

The manuscript was written through contributions of all authors. All authors have given approval to the final version of the manuscript.

Declaration of Competing Interest

The authors declare that they have no known competing financial interests or personal relationships that could have appeared to influence the work reported in this paper.

Data availability

Data will be made available on request.

Acknowledgements

The authors acknowledge funding from the Knut and Alice Wallenberg Foundation (KAW) through the Wallenberg Wood Science Center. The authors acknowledge DESY (Hamburg, Germany), a member of the Helmholtz Association HGF, for the provision of experimental facilities. Parts of this research were carried out at beamline P03 of PETRA III. We thank Alisher Kurmanbay (KTH Royal Institute of Technology) for supporting some of the WAXS measurements. We thank Assoc. Prof. Torbjörn Pettersson (KTH Royal Institute of Technology) for helpful discussions on the AFM measurements.

Appendix A. Supplementary data

Supplementary data to this article can be found online at https://doi.org/10.1016/j.eurpolymj.2023.112141.

References

[1] M.A.A. AlMaadeed, D. Ponnamma, A.A. El-Samak, Polymers to improve the world and lifestyle: physical, mechanical, and chemical needs, in: M.A.A. AlMaadeed, D. Ponnamma,M.A. Carignano (Eds.), Polymer Science and Innovative Applications, 2020, pp. 1-19.
[2] D. Ratna, Chemistry and general applications of thermoset resins, in: (Eds.), Recent Advances and Applications of Thermoset Resins, 2022, pp. 1-172.
[3] F. Ng, G. Couture, C. Philippe, B. Boutevin, S. Caillol, Bio-Based Aromatic Epoxy Monomers for Thermoset Materials, Molecules 22 (2017). https://10.3390/molecules22010149.
[4] R.H. Hinton, F.E. Mitchell, A. Mann, D. Chescoe, S.C. Price, A. Nunn, P. Grasso, J. W. Bridges, Effects of phthalic acid esters on the liver and thyroid, Environ Health Perspect 70 (1986) 195–210. https://10.1289/ehp.8670195.
[5] A.M. Nelson, T.E. Long, A perspective on emerging polymer technologies for bisphenol-A replacement, Polym. Int. 61 (2012) 1485–1491. https://10.1002/pi.4323.
[6] R.A. Sheldon, Green and sustainable manufacture of chemicals from biomass: state of the art, Green Chem. 16 (2014) 950–963. https://10.1039/c3gc41935e.
[7] J.J. Bozell, G.R. Petersen, Technology development for the production of biobased products from biorefinery carbohydrates—the US Department of Energy's "Top 10" revisited, Green Chem. 12 (2010). https://10.1039/b922014c.
[8] O. Yu, K.H. Kim, Lignin to Materials: A Focused Review on Recent Novel Lignin Applications, Appl. Sci. 10 (2020). https://10.3390/app10134626.
[9] M. Norgren, H. Edlund, Lignin: Recent advances and emerging applications, Curr. Opin. Colloid Interface Sci. 19 (2014) 409–416. https://10.1016/j.cocis.2014.08.004.
[10] W. Yang, H. Ding, D. Puglia, J.M. Kenny, T. Liu, J. Guo, Q. Wang, R. Ou, P. Xu, P. Ma, P.J. Lemstra, Bio-renewable polymers based on lignin-derived phenol monomers: Synthesis, applications, and perspectives, SusMat 2 (2022) 535–568. https://10.1002/sus2.87.
[11] C. Weng, X. Peng, Y. Han, Depolymerization and conversion of lignin to value-added bioproducts by microbial and enzymatic catalysis, Biotechnol Biofuels 14 (2021) 84. https://10.1186/s13068-021-01934-w.
[12] J.S. Mahajan, R.M. O'Dea, J.B. Norris, L.T.J. Korley, T.H. Epps, Aromatics from Lignocellulosic Biomass: A Platform for High-Performance Thermosets, ACS Sustain. Chem. Eng. 8 (2020) 15072–15096. https://10.1021/acssuschemeng.0c04817.
[13] M. Alherech, S. Omolabake, C.M. Holland, G.E. Klinger, E.L. Hegg, S.S. Stahl, From Lignin to Valuable Aromatic Chemicals: Lignin Depolymerization and Monomer Separation via Centrifugal Partition Chromatography, ACS Cent Sci 7 (2021) 1831–1837. https://10.1021/acscentsci.1c00729.
[14] M. Lawoko, J.S.M. Samec, Kraft lignin valorization: Biofuels and thermoset materials in focus, Curr. Opin. Green Sustainable Chem. 40 (2023). https://10.1016/j.cogsc.2022.100738.
[15] A. Nasrullah, A.H. Bhat, A. Sada Khan, H. Ajab, Comprehensive approach on the structure, production, processing, and application of lignin, in: (Eds.), Lignocellulosic Fibre and Biomass-Based Composite Materials, 2017, pp. 165-178.

[16] N. Zhou, W.P.D.W. Thilakarathna, Q.S. He, H.P.V. Rupasinghe, A. Review, Depolymerization of Lignin to Generate High-Value Bio-Products: Opportunities, Challenges, and Prospects, Front. Energy Res. 9 (2022). https://10.3389/fenrg.2021.758744.
[17] W. Boerjan, J. Ralph, M. Baucher, Lignin biosynthesis, Annu. Rev. Plant Biol. 54 (2003) 519–546. https://10.1146/annurev.arplant.54.031902.134938.
[18] H. Luo, M.M. Abu-Omar, Chemicals From Lignin, in: M.A. Abraham (Ed.), Encyclopedia of Sustainable Technologies, Elsevier, 2017, pp. 573–585.
[19] A. Duval, F. Vilaplana, C. Crestini, M. Lawoko, Solvent screening for the fractionation of industrial kraft lignin, Holzforschung 70 (2016) 11–20. https://10.1515/hf-2014-0346.
[20] V. Ponnuchamy, O. Gordobil, R.H. Diaz, A. Sandak, J. Sandak, Fractionation of lignin using organic solvents: A combined experimental and theoretical study, Int. J. Biol. Macromol. 168 (2021) 792–805. https://10.1016/j.ijbiomac.2020.11.139.
[21] V. Passoni, C. Scarica, M. Levi, S. Turri, G. Griffini, Fractionation of Industrial Softwood Kraft Lignin: Solvent Selection as a Tool for Tailored Material Properties, ACS Sustain. Chem. Eng. 4 (2016) 2232–2242. https://10.1021/acssuschemeng.5b01722.
[22] A. Tagami, C. Gioia, M. Lauberts, T. Budnyak, R. Moriana, M.E. Lindström, O. Sevastyanova, Solvent fractionation of softwood and hardwood kraft lignins for more efficient uses: Compositional, structural, thermal, antioxidant and adsorption properties, Ind. Crop. Prod. 129 (2019) 123–134. https://10.1016/j.indcrop.2018.11.067.
[23] S. Aminzadeh, M. Lauberts, G. Dobele, J. Ponomarenko, T. Mattsson, M. E. Lindström, O. Sevastyanova, Membrane filtration of kraft lignin: Structural charactristics and antioxidant activity of the low-molecular-weight fraction, Ind. Crop. Prod. 112 (2018) 200–209. https://10.1016/j.indcrop.2017.11.042.
[24] O. Sevastyanova, M. Helander, S. Chowdhury, H. Lange, H. Wedin, L.M. Zhang, M. Ek, J.F. Kadla, C. Crestini, M.E. Lindstrom, Tailoring the Molecular and Thermo-Mechanical Properties of Kraft Lignin by Ultrafiltration, J. Appl. Polym. Sci. 131 (2014), https://doi.org/10.1002/app.40799.
[25] T.V. Lourençon, F.A. Hansel, T.A. da Silva, L.P. Ramos, G.I.B. de Muniz, W.L. E. Magalhães, Hardwood and softwood kraft lignins fractionation by simple sequential acid precipitation, Sep. Purif. Technol. 154 (2015) 82–88. https://10.1016/j.seppur.2015.09.015.
[26] S. Laurichesse, L. Avérous, Chemical modification of lignins: Towards biobased polymers, Prog. Polym. Sci. 39 (2014) 1266–1290. https://10.1016/j.progpolymsci.2013.11.004.
[27] L. Zoia, A. Salanti, P. Frigerio, M. Orlandi, Exploring Allylation and Claisen Rearrangement as a Novel Chemical Modification of Lignin, BioResources 9 (2014) 6540–6561. https://10.15376/biores.9.4.6540-6561.
[28] M. Jawerth, M. Johansson, S. Lundmark, C. Gioia, M. Lawoko, Renewable Thiol-Ene Thermosets Based on Refined and Selectively Allylated Industrial Lignin, ACS Sustain. Chem. Eng. 5 (2017) 10918–10925. https://10.1021/acssuschemeng.7b02822.
[29] L.C. Over, M.A.R. Meier, Sustainable allylation of organosolv lignin with diallyl carbonate and detailed structural characterization of modified lignin, Green Chem. 18 (2016) 197–207. https://10.1039/c5gc01882j.
[30] A. Llevot, B. Monney, A. Sehlinger, S. Behrens, M.A.R. Meier, Highly efficient Tsuji-Trost allylation in water catalyzed by Pd-nanoparticles, Chem Commun (Camb) 53 (2017) 5175–5178. https://10.1039/c7cc02380d.
[31] C. Margarita, D. Di Francesco, H. Tuñon, I. Kumaniaev, C.J. Rada, H. Lundberg, Mild and selective etherification of wheat straw lignin and lignin model alcohols by moisture-tolerant zirconium catalysis, Green Chem. (2023). https://10.1039/d2gc04650d.
[32] M.E. Jawerth, C.J. Brett, C. Terrier, P.T. Larsson, M. Lawoko, S.V. Roth, S. Lundmark, M. Johansson, Mechanical and Morphological Properties of Lignin-Based Thermosets, ACS Appl. Polym. Mater. 2 (2020) 668–676. https://10.1021/acsapm.9b01007.
[33] I. Ribca, M.E. Jawerth, C.J. Brett, M. Lawoko, M. Schwartzkopf, A. Chumakov, S. V. Roth, M. Johansson, Exploring the effects of different cross-linkers on lignin-based thermoset properties and morphologies, ACS Sustain. Chem. Eng. 9 (2021) 1692–1702. https://10.1021/acssuschemeng.0c07580.
[34] Iuliana Ribca, B. Sochor, S.V. Roth, M. Lawoko, M.A.R. Meier, M. Johansson. (2023). Effect of molecular organization on the properties of lignin-based thermoset materials [Manuscript submitted for publication].
[35] M. Jawerth, M. Lawoko, S. Lundmark, C. Perez-Berumen, M. Johansson, Allylation of a lignin model phenol: a highly selective reaction under benign conditions towards a new thermoset resin platform, RSC Adv. 6 (2016) 96281–96288. https://10.1039/c6ra21447a.
[36] P. Tomani, The Lignoboost Process, Cell Chem Technol 44 (2010) 53–58.
[37] X. Meng, C. Crestini, H. Ben, N. Hao, Y. Pu, A.J. Ragauskas, D.S. Argyropoulos, Determination of hydroxyl groups in biorefinery resources via quantitative (31)P NMR spectroscopy, Nat. Protoc. 14 (2019) 2627–2647. https://10.1038/s41596-019-0191-1.
[38] Y. Huang, L. Wang, Y. Chao, D.S. Nawawi, T. Akiyama, T. Yokoyama, Y. Matsumoto, Analysis of Lignin Aromatic Structure in Wood Based on the IR Spectrum, J. Wood Chem. Technol. 32 (2012) 294–303. https://10.1080/02773813.2012.666316.
[39] B.-S. Chiou, S.A. Khan, Real-Time FTIR and in Situ Rheological Studies on the UV Curing Kinetics of Thiol-ene Polymers, Macromolecules (1997) 7322–7328, https://doi.org/10.1021/ma9708656.
[40] A. Buffet, A. Rothkirch, R. Dohrmann, V. Korstgens, M.M. Abul Kashem, J. Perlich, G. Herzog, M. Schwartzkopf, R. Gehrke, P. Muller-Buschbaum, S.V. Roth, P03, the microfocus and nanofocus X-ray scattering (MiNaXS) beamline of the PETRA III storage ring: the microfocus endstation, J. Synchrotron Radiat. 19 (2012) 647–653. https://10.1107/S0909049512016895.
[41] B.R. Pauw, A.J. Smith, T. Snow, N.J. Terrill, A.F. Thunemann, The modular small-angle X-ray scattering data correction sequence, J. Appl. Cryst. 50 (2017) 1800–1811. https://10.1107/S1600576717015096.
[42] A.K. Mathew, A. Abraham, K.K. Mallapureddy, R.K. Sukumaran, Lignocellulosic Biorefinery Wastes, or Resources?, in: Thallada Bhaskar, Ashok Pandey, S. Venkata Mohan, Duu-Jong Lee,S.K. Khanal (Eds.), Waste Biorefinery, Elsevier, 2018, pp. 267-297.
[43] M.J. Suota, T.A. da Silva, S.F. Zawadzki, G.L. Sassaki, F.A. Hansel, M. Paleologou, L.P. Ramos, Chemical and structural characterization of hardwood and softwood LignoForce™ lignins, Ind. Crop. Prod. 173 (2021). https://10.1016/j.indcrop.2021.114138.
[44] R. Rinaldi, R. Jastrzebski, M.T. Clough, J. Ralph, M. Kennema, P.C. Bruijnincx, B. M. Weckhuysen, Paving the Way for Lignin Valorisation: Recent Advances in Bioengineering, Biorefining and Catalysis, Angew. Chem. Int. Ed. 55 (2016) 8164–8215. https://10.1002/anie.201510351.
[45] C. Li, X. Zhao, A. Wang, G.W. Huber, T. Zhang, Catalytic Transformation of Lignin for the Production of Chemicals and Fuels, Chem. Rev. 115 (2015) 11559–11624. https://10.1021/acs.chemrev.5b00155.
[46] R. Li, X. Wang, Q. Lin, F. Yue, C. Liu, X. Wang, J. Ren, Structural Features of Lignin Fractionated From Industrial Furfural Residue Using Alkaline Cooking Technology and Its Antioxidant Performance, Front. Energy Res. 8 (2020). https://10.3389/fenrg.2020.00083.
[47] O. Faix, Classification of Lignins from Different Botanical Origins by FT-IR Spectroscopy, Holzforschung 45 (1991) 21–28. https://doi:10.1515/hfsg.1991.45.s1.21.
[48] P.I.F. Pinto, S. Magina, E. Budjav, P.C.R. Pinto, F. Liebner, D. Evtuguin, Cationization of Eucalyptus Kraft LignoBoost Lignin: Preparation, Properties, and Potential Applications, Ind. Eng. Chem. Res. 61 (2022) 3503–3515. https://10.1021/acs.iecr.1c04899.
[49] K. Komisarz, T.M. Majka, K. Pielichowski, Chemical and Physical Modification of Lignin for Green Polymeric Composite Materials, Materials 16 (2022). https://10.3390/ma16010016.
[50] Z. Söyler, M.A.R. Meier, Sustainable functionalization of cellulose and starch with diallyl carbonate in ionic liquids, Green Chem. 19 (2017) 3899–3907. https://10.1039/c7gc01978e.
[51] C.A. Hunter, J.K.M. Sanders, The Nature of π-π Interactions, J. Am. Chem. Soc. 112 (1990) 5524–5534. https://10.1021/ja00170a016.
[52] M.O. Sinnokrot, E.F. Valeev, C.D. Sherrill, Estimates of the ab initio limit for pi-pi interactions: the benzene dimer, J. Am. Chem. Soc. 124 (2002) 10887–10893. https://10.1021/ja025896h.
[53] T. Chen, M. Li, J. Liu, π–π Stacking Interaction: A Nondestructive and Facile Means in Material Engineering for Bioapplications, Cryst. Growth Des. 18 (2018) 2765–2783. https://10.1021/acs.cgd.7b01503.
[54] O. Merino, R. Cerón-Camacho, R. Luque, R. Martínez-Palou, Microwave-Assisted Lignin Solubilization in Protic Ionic Compounds Containing 2,3,4,5-Tetraphenyl-1H-imidazolium and Inorganic Anions, Waste Biomass Valoriz. 11 (2019) 6585–6593. https://10.1007/s12649-019-00916-2.
[55] T. Hatakeyama, H. Hatakeyama, Temperature-Dependence of X-Ray Diffractograms of Amorphous Lignins and Polystyrenes, Polymer 23 (1982) 475–477. https://10.1016/0032-3861(82)90357-3.
[56] C. Gioia, M. Colonna, A. Tagami, L. Medina, O. Sevastyanova, L.A. Berglund, M. Lawoko, Lignin-Based Epoxy Resins: Unravelling the Relationship between Structure and Material Properties, Biomacromolecules 21 (2020) 1920–1928. https://10.1021/acs.biomac.0c00057.